# Endothelial *Cdkn1a* (*p21*) Overexpression and Accelerated Senescence in a Mouse Model of Fuchs Endothelial Corneal Dystrophy

*Mario Matthaei,*[1,2] *Huan Meng,*[1] *Alan K. Meeker,*[3,4] *Charles G. Eberhart,*[1,3,4] *and Albert S. Jun*[1]

**Purpose.** Stress of the endoplasmic reticulum and oxidative stress play critical roles in the pathogenesis of Fuchs Endothelial Corneal Dystrophy (FECD). In the normal aging cornea, cellular stress has been associated with a loss in proliferative capacity (premature senescence) of corneal endothelial cells (CECs). The present study used a transgenic *Col8a2*$^{Q455K/Q455K}$ knock-in mouse model of early-onset FECD to identify the endothelial expression profile of specific cellular stress response–related targets, which may be relevant to late-onset FECD.

**Methods.** The differential endothelial mRNA levels of cellular stress response–related genes were determined in 12-month-old homozygous *Col8a2*$^{Q455K/Q455K}$ mutant and wild-type mice using customized PCR arrays. Result validation and analysis of additional senescence-related transcripts was performed by real-time PCR. Expression of p53 and p21 was assessed by immunofluorescence. Senescence-associated β-galactosidase (SA-β-Gal) activity was investigated by histochemical labeling. Human FECD samples and normal controls were examined for p21 expression by immunohistochemistry.

**Results.** PCR-array analysis showed greater than 2-fold and/or significantly altered endothelial regulation of 19 cellular stress response-related transcripts in *Col8a2*$^{Q455K/Q455K}$ mutant mice; real-time PCR documented statistically significant upregulation of senescence-associated targets *Cdkn1a* (*p21*), *Serpine1* (*PAI-1*), *Tagln* (*Sm22*), *Fn1* and *Clu* (*ApoJ*). Immunofluorescence revealed increased expression of nuclear p53 and p21 in mutant animals. SA-β-Gal staining detected increased proportions of senescent CECs in mutant mice. Human FECD endothelium exhibited increased levels of nuclear p21 protein.

**Conclusions.** Our results identify endothelial *Cdkn1a* (*p21*) upregulation in a mouse model of early-onset FECD, confirm overexpression of p21 in late-onset human FECD endothelium, and suggest a role for premature senescence in FECD. (*Invest Ophthalmol Vis Sci.* 2012;53:6718–6727) DOI:10.1167/iovs-12-9669

Fuchs endothelial corneal dystrophy (FECD) is characterized by progressive loss of corneal endothelial cells (CEC) over several decades. CECs lose their uniform hexagonal structure and undergo a gradual flattening accompanied by thickening of Descemet membrane and formation of posterior excrescences (guttae). The reduced capacity of the endothelium to maintain corneal deturgescence eventually causes stromal edema and loss of vision in advanced stages of the disease. Multiple genes and chromosomal loci associated with FECD have been identified.[1–8] Moreover, molecular studies analyzing potential mechanisms of FECD indicate that oxidative stress and endoplasmic reticulum stress play critical pathogenetic roles.[9–12]

Human CECs do not normally proliferate in vivo, although they are capable of dividing in vitro under optimized conditions. Prolonged periods of subcytotoxic stress may cause a loss of mitotic capacity known as stress-induced premature senescence (SIPS).[13] Compared with "replicative senescence," which is marked by irreversible growth arrest in normal cells after a limited number of mitoses, SIPS is characterized by similar cellular features that are not primarily caused by a shortening of telomeres. Mimura and Joyce found corneal topography and age-related differences in the proliferative capacity of normal HCECs.[14] Studies from the same laboratory reported that oxidative nuclear DNA damage rather than telomere shortening contributes to loss of proliferative capacity in the central corneal endothelium of older donors suggesting involvement of SIPS.[15,16]

We generated a transgenic mouse model for FECD harboring a point mutation homologous to the human FECD-associated Q455K *COL8A2* mutation, which exhibits a phenotype strikingly similar to human FECD.[12] Compared with human end-stage corneas with FECD retrieved at transplantation, this mouse model provides the opportunity to investigate tissues from earlier stages of the disease under highly standardized conditions. Results from such studies can then be correlated with human late-onset FECD tissues at a more advanced disease stage obtained at keratoplasty. One potential advantage of this approach is the possibility of identifying cellular changes that may be relevant to understanding both early- and late-onset disease and to developing future nonsurgical treatment approaches.

Using this model, the present study examined the stress response of CECs in both mutant and wild-type animals. PCR-array based gene-profiling indicated upregulation of the senescence associated marker cyclin-dependent kinase inhibitor 1A (*Cdkn1a/p21*). Hypothesizing that SIPS may play a role

From [1]The Wilmer Eye Institute, Johns Hopkins Medical Institutions, Baltimore, Maryland; the [2]Department of Ophthalmology, University Medical Center Hamburg-Eppendorf, Hamburg, Germany; the [3]Sidney Kimmel Comprehensive Cancer Center, Johns Hopkins Medical Institutions, Baltimore, Maryland; and the [4]Department of Pathology, Johns Hopkins Medical Institutions, Baltimore, Maryland.

Supported by Deutsche Forschungsgemeinschaft DFG MA 5110/2-1 (MM); National Institutes of Health Grants EY019874 (ASJ) and EY001765 (to Wilmer Microscopy Core Facility); Medical Illness Counseling Center (ASJ); and Research to Prevent Blindness (to The Wilmer Eye Institute).

Submitted for publication February 9, 2012; revised July 18, 2012; accepted August 31, 2012.

Disclosure: **M. Matthaei**, None; **H. Meng**, None; **A.K. Meeker**, None; **C.G. Eberhart**, None; **A.S. Jun**, None

Corresponding author: Albert S. Jun, The Wilmer Eye Institute, 400 North Broadway, Baltimore, MD 21231; aljun@jhmi.edu.

in the pathogenesis of FECD, we confirmed our findings by analyzing additional SIPS associated genes and senescence-associated–β–galactosidase (SA-β-Gal) staining in mutant and wild-type mice. We subsequently confirmed nuclear p21 overexpression in genetically undifferentiated, late-onset human FECD CECs compared with normal endothelium. The novel results presented here suggest involvement of p21-overexpression and SIPS in the pathogenesis of FECD.

## Materials and Methods

### Animals

Homozygous wild-type (WT) and *Col8a2*$^{Q455K/Q455K}$ mutant (MUT) mice of various ages were used for all described animal studies.[12] Animals were maintained under specific pathogen-free conditions in accordance with the ARVO Statement for the Use of Animals in Ophthalmic and Vision Research and adhering to protocols approved and monitored by the Animal Care and Use Committee of The Johns Hopkins University.

### Human Tissue

Studies using human tissues were approved by The Johns Hopkins Institutional Review Board and adhered to the tenets of the Declaration of Helsinki. Ten formalin-fixed and paraffin–embedded, penetrating keratoplasty specimens for FECD ($n = 5$) or normal autopsy whole globes ($n = 5$) were collected from the Wilmer Eye Pathology Service or the Johns Hopkins Hospital Autopsy Service. Demographic information of tissue donors is presented in Table 1.

### Clinical Confocal Microscopy

Clinical confocal microscopy was performed as previously described.[12] A confocal microscope (ConfoScan3; Nidek, Fremont, CA) with a 40× objective was used. Mice were anesthetized by spontaneous inhalation of isoflurane (Vedco, St. Joseph, MO) and euthanized by cervical dislocation. Approximately 100 images of the central corneal endothelium were recorded. Endothelial cell densities were calculated from randomly selected pictures using imaging software (Nidek).

### PCR Arrays

Mice were anesthetized and euthanized as described above. After clinical confocal microscopy, both eyes were extracted, corneal buttons were excised, and Descemet membranes were stripped under a dissecting microscope using jeweler's forceps. Four Descemet membranes from two 12-month-old mice of the same strain (WT or MUT) were pooled per group. Total RNA isolation was performed from CECs from three groups per strain using TRIzol reagent (Invitrogen, Carlsbad, CA) and subsequent RNeasy (Qiagen, Valencia, CA) column purification. RNA yield was measured with a spectrophotometer (NanoDrop 2000; Thermo Scientific, Waltham, MA). Total RNA was reverse transcribed to cDNA using a reverse transcription kit (High Capacity cDNA Reverse Transcription Kit; Applied Biosystems, Foster City, CA). cDNA was preamplified using a master mix (TaqMan PreAmp Master Mix; Applied Biosystems) and a customized PreAmp Pool (Applied Biosystems). The preamplification product and master mix (Universal Master Mix II, no UNG; Applied Biosystems) were loaded onto well plates (Custom TaqMan Array Plates; Applied Biosystems) and run on a real-time PCR instrument (StepOne Plus Cycler; Applied Biosystems) according to manufacturer's instructions. The array plates included a customized panel of 96 genes (see Supplementary Material and Supplementary Table S1, http://www.iovs.org/lookup/suppl/doi:10.1167/iovs.12-9669/-/DCSupplemental) based on another commercially available array (Stress & Toxicity Pathway Finder PCR Array; SABiosciences, Frederick, MD). The expression of each gene was normalized to the average expression of 18S ribosomal RNA (*18S*), beta-actin (*Actb*), beta-glucuronidase (*Gusb*), and hypoxanthine guanine phosphoribosyl transferase (*Hprt1*). Relative gene expression in endothelial cells of MUT compared with WT corneas was calculated using data analysis software (DataAssist Software v3.0; Applied Biosystems).

### Indirect Immunofluorescence of Corneal Flatmounts

MUT and WT mice were euthanized, and FECD or normal phenotype was confirmed by clinical confocal microscopy. Corneoscleral buttons were excised, fixed for 30 minutes in 0.5% paraformaldehyde, and permeabilized for 15 minutes in 0.5% nonionic surfactant solution (Triton-X; Sigma-Aldrich, St. Louis, MO). Blocking of nonspecific binding sites was performed for 30 minutes in 5% goat serum. Primary and secondary antibodies were diluted in 2% BSA and applied for 1 hour at 37°C. 4′,6-diamidino-2-phenylindole (DAPI, 1:1000, Invitrogen) was added to the diluted secondary antibodies as nuclear counterstain. Four radial incisions were made and the bowl-shaped tissues were flatmounted in antifade reagent (ProLong Gold; Invitrogen).

The primary antibodies used were: rabbit anti-mouse p21 (ab2961, concentration 1:20, Abcam, Cambridge, MA); rabbit anti-mouse p53 (CM5, concentration 1:100, Novocastra, Newcastle, UK); and mouse antimouse or rabbit antimouse ZO-1 (ZO1-1A12 or ZO-1(MID),

**Table 1.** Donor Information for Human Autopsy (A) and Fuchs Dystrophy (B) Tissue Specimens

| Autopsy Eyes (A) | | | |
|---|---|---|---|
| **Age** | **Sex** | **Cause of Death** | **Corneal Findings** |
| 71 | F | Cerebral infarction | Normal |
| 75 | F | Rupture of aneurysm | Normal |
| 77 | M | Pulmonary alveolar hemorrhage | Normal |
| 84 | F | Myocardial infarction | Normal |
| 90 | F | Bronchitis | Normal |
| 79.4 ± 3.4 (Mean ± SEM) | | | |
| **Fuchs Dystrophy Corneas (B)** | | | |
| **Age** | **Sex** | **Clinical Diagnosis** | **Pathological Diagnosis** |
| 72 | F | Fuchs dystrophy | Fuchs dystrophy |
| 75 | F | Fuchs dystrophy | Fuchs dystrophy |
| 76 | M | Fuchs dystrophy | Fuchs dystrophy |
| 83 | M | Fuchs dystrophy | Fuchs dystrophy |
| 87 | F | Fuchs dystrophy | Fuchs dystrophy |
| 78.6 ± 2.8 (Mean ± SEM) | | | |

concentration 1:200, Invitrogen). Secondary antibodies used were goat anti-rabbit IgG (Alexa Fluor 488 Goat Anti-Rabbit IgG, concentration 1:500, Invitrogen) and goat anti-mouse IgG (Alexa Fluor 555 Goat Anti-Mouse IgG, concentration 1:500; Invitrogen). Images were obtained with a confocal microscope and software (LSM 510 META; Zeiss, Thornwell, NY) using a 40× oil-immersion objective and 2× digital zoom.

Immunolabeling for ZO-1 protein and nuclear counterstaining with DAPI were used to identify multinucleated CECs. Proportionate quantification of multinucleated CECs and p21 or p53 positive nuclei was performed by calculating the mean ± SEM of the respective cells or nuclei in three microscopic visual fields per cornea at 400× magnification.

## Real-Time PCR

RNA was extracted from three to six groups of WT and MUT mice at 5 months (one Descemet membrane from an individual animal per "group") and 12 months (four Descemet membranes from two animals per group), respectively. RNA was transcribed to cDNA as described above. Preamplification was performed using a preamp (Applied Biosystems) and inventoried gene expression assays (Applied Biosystems). Real-time PCR was conducted on a PCR system (Applied Biosystems) using a master mix and inventoried gene expression assays (Applied Biosystems). Assays (Applied Biosystems) used were Mm00607939_s1 (*Actb*); Mm00432359_m1 (cyclin D1 [*Ccnd1*]); Mm00432448_m1 (*Cdkn1a*); Mm00494449_m1 (cyclin-dependent kinase inhibitor 2A [*Cdkn2a*]); Mm00442773_m1 (clusterin [*Clu*]), Mm00432936_m1 (E2F transcription factor 1 [*E2f1*]); Mm00656724_m1 (early growth response 1 [*Egr1*]); Mm01256744_m1 (fibronectin 1 [*Fn1*]); Mm00516005_m1 (heme oxygenase [decycling] 1 [*Hmox1*]); Mm00485586_m1 (retinoblastoma 1 [*Rb1*]); Mm00435860_m1 (serine [or cysteine] peptidase inhibitor, clade E, member 1 [*Serpine1*]); and Mm00441661_g1 (transgelin [*Tagln*]). Expression of each target gene was normalized to the average expression of *Actb*. The comparative CT method was applied to calculate relative gene expression.

## Senescence-Associated Beta-Galactosidase Staining and Evaluation

The assessment of senescence-associated beta-galactosidase (SA-β-Gal) activity in the corneal endothelium of 5-month-old ($n = 3$ per strain) and 14-month-old ($n = 4$ per strain) MUT and WT mice was performed using a commercial senescence detection kit (Cell Signaling, Danvers, MA). Globes of euthanized animals were extracted and washed in PBS. Whole eyes were fixed for 5 minutes in 2% formaldehyde and 0.2% glutaraldehyde in PBS. Corneoscleral buttons were excised and re-fixed in fixative solution for 5 minutes. This was followed by washing in PBS and incubation in β-GAL staining solution at 37°C overnight according to manufacturer's instructions. The staining was performed at pH 5.5 to increase its sensitivity. Corneas stained at pH 4.0 were used as positive controls. Subsequently, corneoscleral buttons were washed in PBS and cryopreserved in OCT (Sakura, Torrance, CA) at −80°C. Cryosections of 4 μm were placed on Superfrost Plus Slides and air-dried at room temperature. Tissue sections were stained with Nuclear Fast Red (Sigma) and cover-slipped with a mounting medium (CytoSeal 60; Thermo Scientific).

Four nonoverlapping sections per specimen were evaluated under a light microscope using 400× magnification. Each endothelial cell was graded according to a classification described previously and dividing the SA-β-Gal staining intensities into four categories (0, no staining; 1, weak focal staining; 2, moderate multifocal staining; 3, intense multifocal staining).[14]

## Immunohistochemistry

Sections measuring 4-μm in thickness from paraffin-embedded tissue samples of human FECD corneas or autopsy eyes were preheated at 65°C for 60 minutes. Sections were deparaffinized in three 5-minute washes of Xylene and hydrated in graded ethanol. Heat-mediated antigen retrieval was performed for 60 minutes in a modified citrate buffer (Target Retrieval Solution; DAKO, Carpinteria, CA). Dual enzyme block solution (DAKO) was used for 10 minutes at room temperature to block unspecific tissue enzyme activity. Mouse anti-human p21 IgG (Clone 6B6, concentration 1:50; BD Biosciences, Franklin Lakes, NJ) was used as primary antibody and applied at 4°C overnight. Tissue-bound primary antibody was detected by incubation with an anti-Mouse IgG reagent (Power Vision Poly-HRP; Leica Microsystems, Buffalo Grove, IL) for 30 minutes and subsequent developing in filtered diaminobenzidine (DAB) chromogen solution (Sigma Fast DAB tablet set, Sigma). Nuclei were briefly counterstained with 1:5 Mayer's hematoxylin (DAKO) in distilled $H_2O$ and tissue sections dehydrated in ethanol gradients and xylene, reversing the hydration steps described above. Sections were cover-slipped with mounting medium (Vector Laboratories, Burlingame, CA) and the percentage of p21-positive nuclei from one whole section was evaluated under a light microscope using a 100× oil-immersion objective.

## Statistics

The unpaired, two-tailed *t*-test was applied using statistical software (PRISM4; GraphPad, La Jolla, CA). $P < 0.05$ was considered statistically significant.

# Results

## Clinical Confocal Microscopy and Quantification of Multinucleated Cells

Clinical confocal microscopy was performed to confirm the FECD phenotype in all MUT animals and the normal endothelial phenotype in WT animals. The endothelial cell density in 5-month MUT and WT mice ($n = 3$ per strain) was 1454 ± 92/mm$^2$ (mean value ± SEM) and 2035 ± 66/mm$^2$, respectively; and for 12-month MUT and WT mice ($n = 8$ per strain) 1071 ± 50/mm$^2$ and 2109 ± 34/mm$^2$, respectively (Fig. 1). As stated in a previous report from our laboratory, CECs in all 5- and 12 month-old mutant animals showed increased variation in cellular shape (pleomorphism) and size (polymegethism).[12] Furthermore, we observed hyperreflective endothelial nuclei and scattered multinucleated cells (Fig. 1). Immunofluorescence labeling of ZO-1 and nuclear counterstaining with DAPI demonstrated an increased proportion of multinucleated cells in 10-month-old MUT compared with WT animals ($n = 3$, $P < 0.05$; Fig. 1). These morphologic changes suggested similarities between CECs in our animal model and senescent cells. Typical morphologic features of senescent cells include an enlarged and irregular shape with loss of cytoplasm and the appearance of multiple nuclei.[17]

## PCR Array and Real-Time PCR Validation

Expression could be detected for 90 out of 96 genes (93.8%) on the customized PCR arrays. Eight genes (8.3%) showed endothelial overexpression in MUT mice greater than 2-fold (Fig. 2, *red*); and eight transcripts (8.3%) were more than 2-fold downregulated compared with WT mice (Fig. 2, *green*). A total of nine transcripts (9.4%) showed a statistically significant difference in MUT compared with WT mice ($P < 0.05$) (Fig. 2A, above horizontal dashed line). A detailed list of genes with greater than 2-fold and/or statistically significant differential expression and their assignment to functional groups is presented in Table 2. Functional group and relative gene expression values for all genes investigated are provided in Supplementary Table S1 (see Supplementary Material and

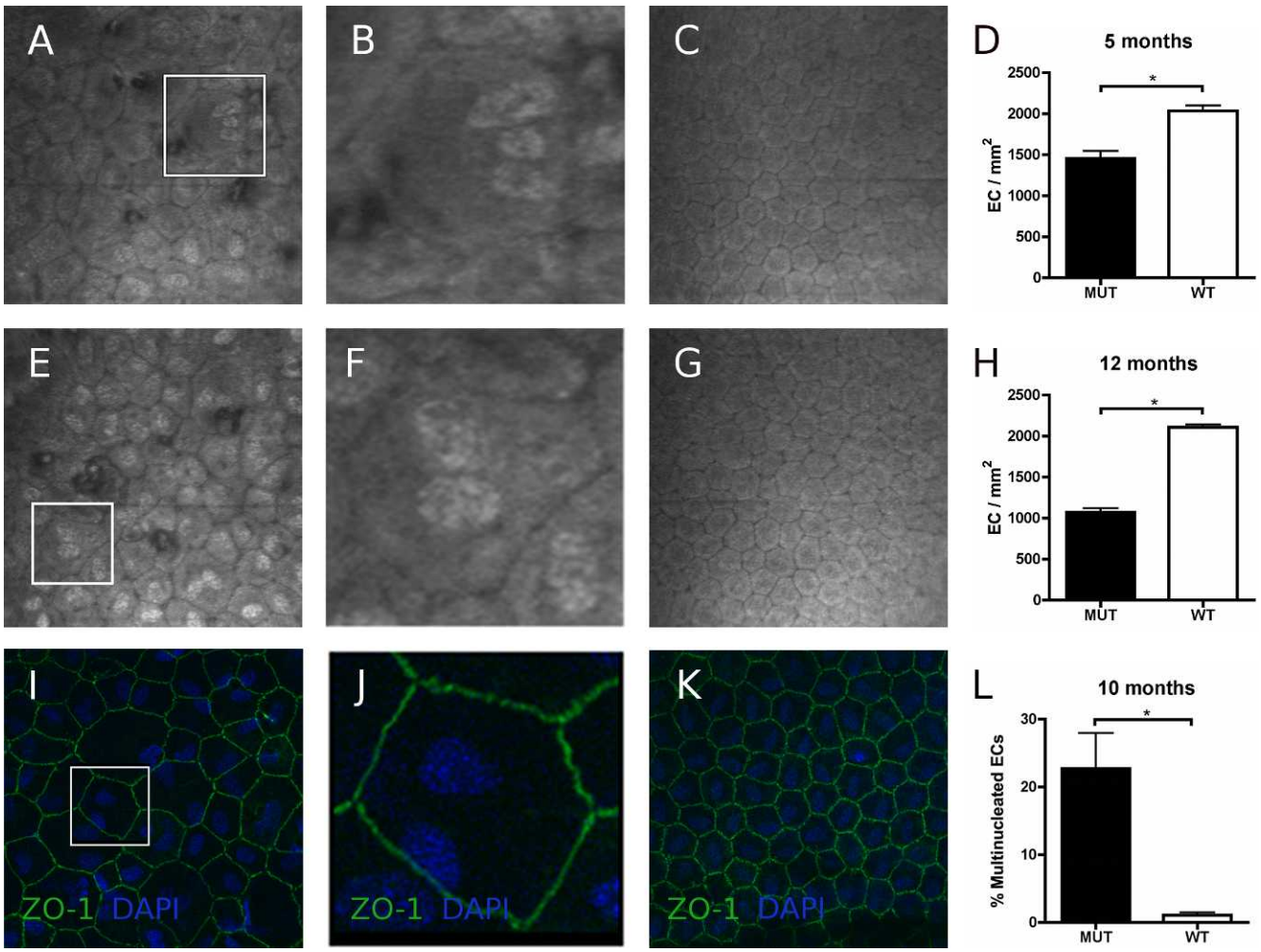


**Figure 1.** Endothelial Imaging of *Col8a2* $^{Q455K/Q455K}$ MUT and WT mice. Analysis of clinical confocal microscopy images indicated irregularity of shape (pleomorphism) and cell size (polymegethism) in MUT mice at 5 months (**A**) along with scattered guttae, hyperreflectivity of nuclei, and incidence of multinucleated cells (**B**, shows magnified box from **A**). No such changes were observed in WT mice at 5 months (**C**). Corneal endothelium of 12 month-old MUT mice showed progression of the FECD phenotype (**E**, **F**; **F** shows magnified box from **E**). WT endothelium at same age presented virtually unchanged (**G**). Statistically significant loss of endothelial cell(EC) density was confirmed in MUT compared with WT mice at 5 months (**D**) and 12 months (**H**) as previously reported.[12] Endothelial immunofluorescence labeling of zonula-1 (ZO-1, *green*) and DAPI (*blue*) counterstaining in 10 month-old MUT (**I**, **J**; **J** shows magnified box from **I**) and WT (**K**) animals confirmed an increased proportion of multinucleated cells in MUT animals (**L**). Data are mean ± SEM. $^*P < 0.05$.

Supplementary Table S1, http://www.iovs.org/lookup/suppl/doi:10.1167/iovs.12-9669/-/DCSupplemental).

Selected genes from the PCR arrays were validated by real-time PCR in sets of mice at two different ages as presented in Figure 2. The mean fold-changes (± SEM) for each gene expressed in MUT compared with WT mice at 5/12 months, respectively, were: *Cdkn1a* (p21) 2.2 ± 0.57 / 3.2 ± 0.5*; *Ccnd1* 2.5 ± 0.2* / 6.1 ± 0.6*; *E2f1* 3.2 ± 1.0 / 2.3 ± 0.2*; *Egr1* 11.9 ± 1.0* / 23.5 ± 7.8*; and *Hmox1* 6.6 ± 0.7* / 5.2 ± 0.6* (*$P < 0.05$). These data correlated well with the data from the PCR arrays and showed an even higher differential expression in 12-month-old MUT mice for *Cdkn1a* (p21) and *Egr1*.

## Nuclear p53 and p21 Expression and Real-Time PCR Expression Analysis of Additional Senescence-Related Genes

The following experiments focused on the investigation of a potential involvement of endothelial premature senescence in FECD. The p21 protein (encoded by *Cdkn1a*) may exert different functions depending on its cellular localization. Nuclear expression of p21 has previously been shown in human and mouse CECs and is associated with inhibition of cell cycle progression and cellular senescence.[17–19] We therefore first verified the nuclear localization of the p21 protein and its transcription factor p53 by immunofluorescence and analyzed their expression levels (Fig. 3). Increased proportions of p53 and p21 positive endothelial nuclei were observed in the corneal endothelium of 14 month-old MUT compared with WT animals (four eyes from two animals per group, Fig. 3). Subsequently, an additional panel of senescence-associated genes, including targets that previously have shown differential expression in prematurely senescent cells of other ocular tissues, was examined in the corneal endothelium of 5- and 12-month MUT and WT mice.[20,21] We found statistically significant upregulation in MUT endothelium of one out of six genes at 5 months and of four out of six genes at 12 months (Fig. 4). Transcript levels for each gene expressed in MUT compared with WT mice at the ages of 5/12 months, respectively, were (mean ± SEM) *Cdkn2a* 1.3 ± 0.1 / 0.7 ± 0.3; *Clu* 2.0 ± 0.1* / 1.3 ± 0.0*; *Fn1* 1.4 ± 0.1 / 1.5 ± 0.1*;

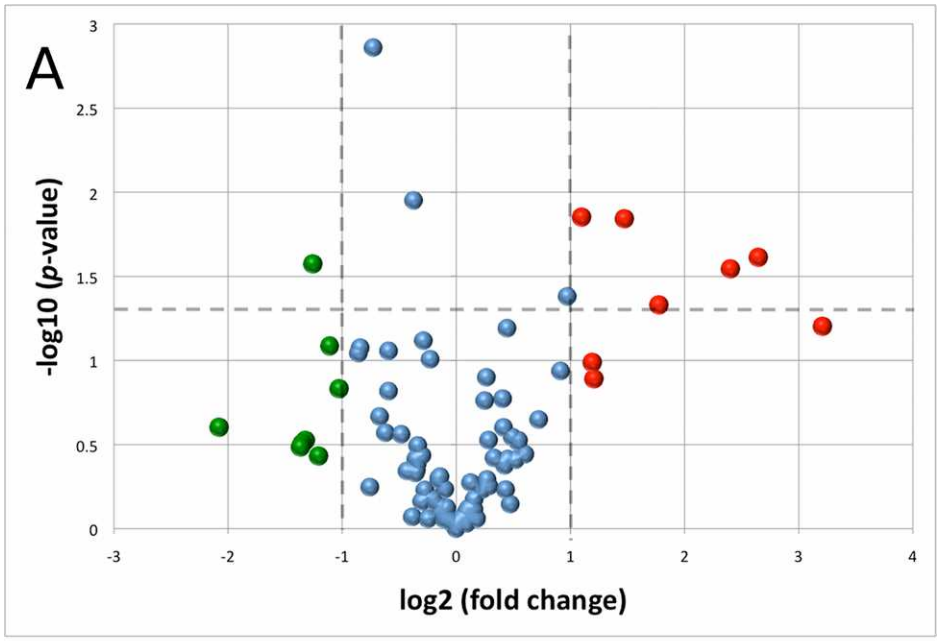


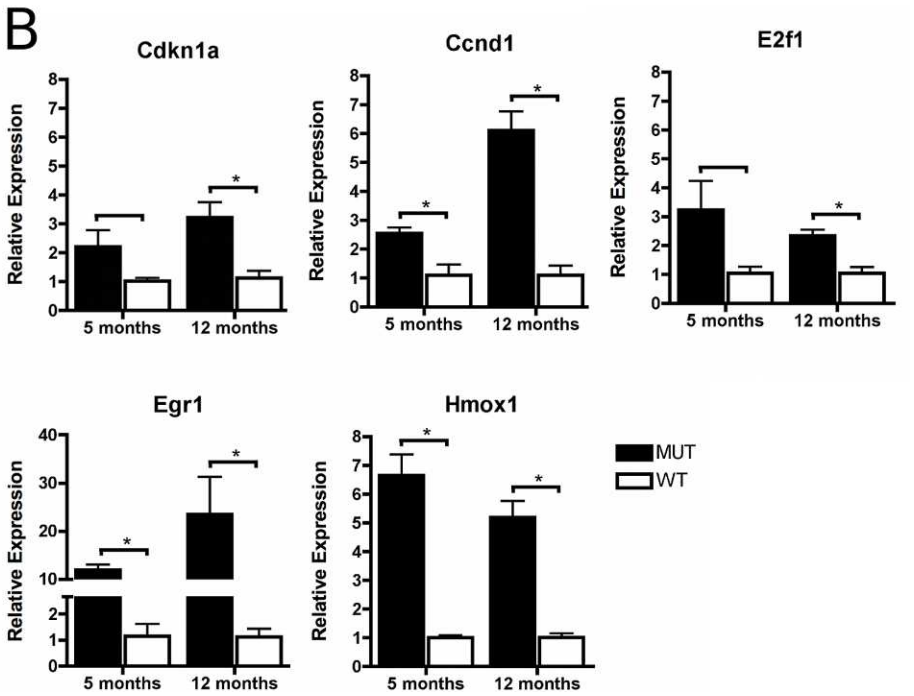


**Figure 2.** PCR array analysis and validation. (**A**) PCR array analysis of cellular stress related genes in 12 month-old groups of *Col8a2* $^{Q455K/Q455K}$ MUT and WT mice ($n = 3$): Gene expression was normalized to the mean expression level of *18S*, *Actb*, *Gusb*, and *Hprt1*. Eight genes showed greater than 2-fold transcriptional upregulation (*red*) or downregulation (*green*). A statistically significant (above $P = 0.05$, marked by *horizontal dashed line*) difference was noted in nine genes. (**B**) Validation of gene array data was performed by real-time PCR analysis of selected genes in MUT and WT mice at 5 and 12 months of age, target gene expression was normalized to mean expression of *Actb*. Data are mean ± SEM. *$P < 0.05$.

*Rb1* 1.2 ± 0.2 / 0.8 ± 0.1; *Serpine1* 1.9 ± 0.1 / 7.0 ± 1.6*; and *Tagln* 1.8 ± 0.3 / 2.5 ± 0.3* (*$P < 0.05$).

## SA-β-Gal Staining

SA-β-Gal staining is a broadly accepted approach to detect senescent cells.[22] It is based on increased lysosomal content of senescent cells that can still be detected at a suboptimal pH.[23] We performed endothelial SA-β-Gal staining of 5- and 14-month MUT and WT mice. The percentage of SA-β-Gal positive CECs in WT mice (mean ± SEM) was 4.6 ± 0.7 % at 5 months and 15.4 ± 5.9 % at 14 months. A statistically significant ($P < 0.05$) increased percentage of SA-β-Gal positive CECs was evident in MUT mice at both timepoints exhibiting 18.3 ± 1.3 % and 58.8 ± 3.7 % SA-β-Gal positive CECs at 5 months and 14 months, respectively (Fig. 5).

**Table 2.** Differentially Expressed Genes on PCR Arrays

| Gene | Functional Group | Fold Change | *P* Value |
|---|---|---|---|
| **Egr1** | **Proliferation and carcinogenesis** | **9.28** | **0.06** |
| **Ccnd1** | **Proliferation and carcinogenesis** | **6.28** | **0.02** |
| **Hmox1** | **Oxidative and metabolic stress** | **5.30** | **0.03** |
| **E2f1** | **Proliferation and carcinogenesis** | **3.43** | **0.05** |
| Ung | DNA Damage and repair | 2.78 | 0.01 |
| **Cdkn1a** | **Growth arrest and senescence** | **2.31** | **0.13** |
| Fasl | Apoptosis signaling | 2.29 | 0.10 |
| Ddit3 | UPR/growth arrest and senescence | 2.14 | 0.01 |
| Hspa5 | UPR/heat shock | 1.96 | 0.04 |
| Hspa4 | Heat shock | −1.29 | 0.01 |
| Xrcc2 | DNA damage and repair | −1.65 | 0.00 |
| Gstm1 | Oxidative and metabolic stress | −2.03 | 0.15 |
| Ephx2 | Oxidative and metabolic stress | −2.15 | 0.08 |
| Cyp2b10 | Oxidative and metabolic stress | −2.30 | 0.37 |
| Hspa1l | UPR/heat shock | −2.38 | 0.03 |
| Gpx2 | Oxidative and metabolic stress | −2.49 | 0.30 |
| Cyp4a10 | Oxidative and metabolic stress | −2.54 | 0.31 |
| Cyp2c29 | Oxidative and metabolic stress | −2.57 | 0.33 |
| Ero1lb | UPR | −4.22 | 0.25 |

The list presents genes with more than 2-fold change and/or $P < 0.05$ in 12–month-old *Col8a2* $^{Q455K/Q455K}$ MUT mice compared with WT mice. Fold-change >1 indicates overexpression and fold-change <−1.0 indicates underexpression in MUT compared with WT mice. Differential expression of bold genes was validated by real-time PCR.

## Immunohistochemistry for p21 in Human Samples

Immunolabeling of the p21 protein in human corneas showed higher staining intensity and a statistically significant ($P < 0.05$) increase in the percentage (FECD 41.3 ± 14.3 % (mean ± SEM versus autopsy 6.1 ± 2.6 %) of p21-positive nuclei in the endothelium of FECD patients compared with normal autopsy cases (Fig. 6). The total number (mean ± SEM) of

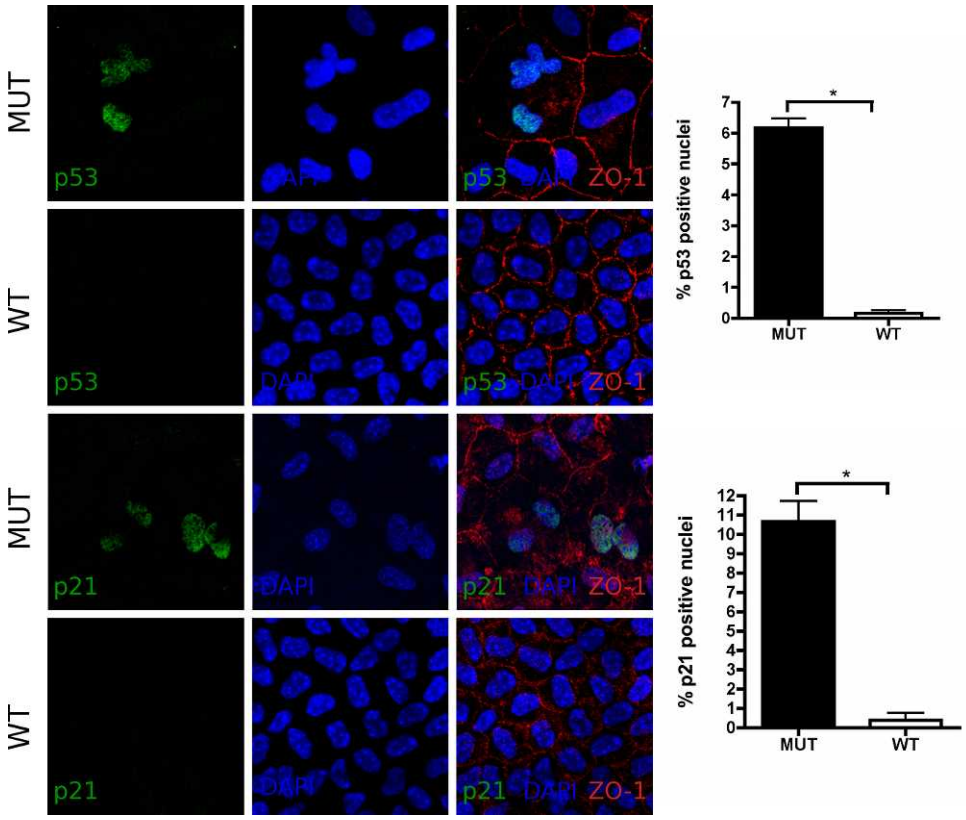


**Figure 3.** Immunofluorescence in corneal flatmounts of 10 month-old *Col8a2* $^{Q455K/Q455K}$ MUT and WT mice: Increased proportions of p53 (*green*, top and second row) and p21 (*green*, third and bottom row) positive nuclei were detected in MUT animals compared with WT controls. Nuclei were counterstained with DAPI (*blue*) and cell borders were immunolabeled with antibody to ZO-1 (*red*). Magnification 800×; data are mean ± SEM. *$P < 0.05$.

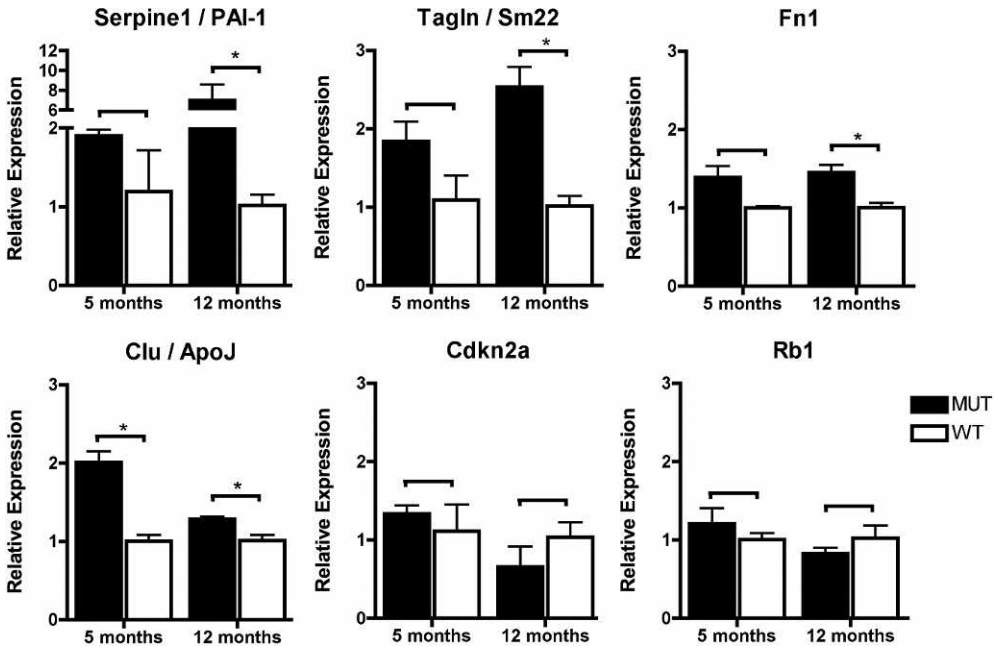


**Figure 4.** Relative expression of an additional set of senescence associated genes in *Col8a2* $^{Q455K/Q455K}$ MUT compared with WT mice at 5 and 12 months of age. Real-time PCR analysis was performed for each group, and target gene expression was normalized to mean expression of *Actb*. Data are mean ± SEM. $^{*}P < 0.05$.

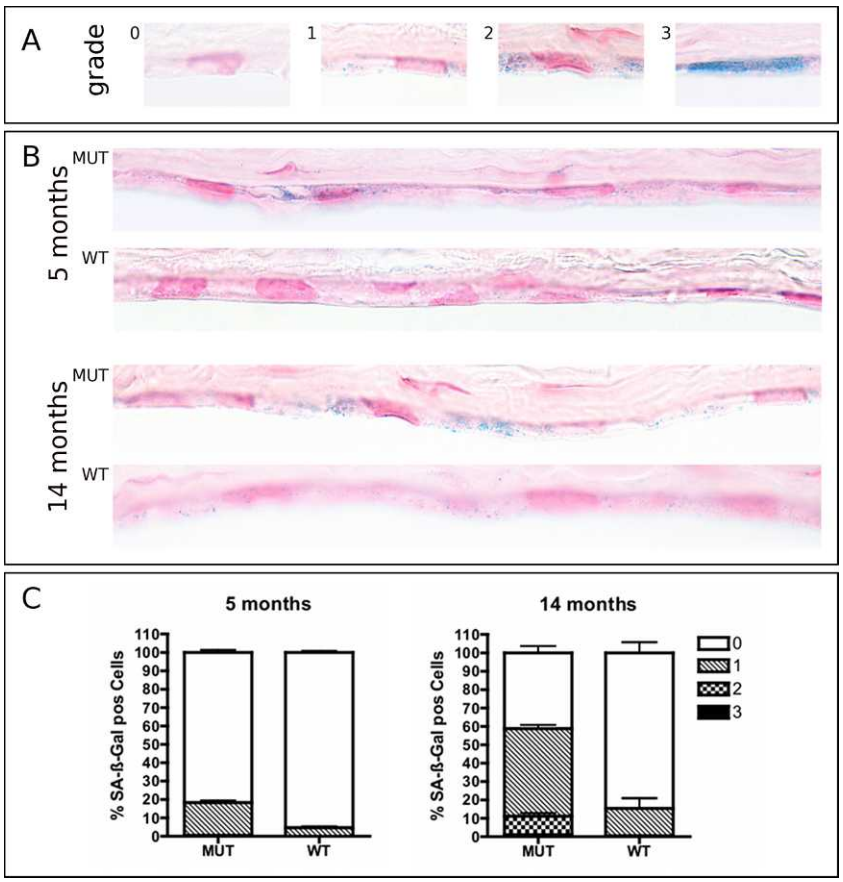


**Figure 5.** SA-β-Gal staining of corneoscleral buttons from 5- and 14-month-old *Col8a2* $^{Q455K/Q455K}$ MUT and WT mice (pH 5.5). Cryosections were counterstained with nuclear fast red. (**A**) Staining intensity was graded according to a scoring system previously described by Mimura and Joyce[14]: 0, no staining; 1, focal weak staining; 2, multifocal moderate staining; or 3, multifocal intense staining. (**B**) Increased staining intensity was noted in sections of MUT compared with WT mice accumulating with age in both strains. (**C**) Diagrams depict proportions of corneal endothelial cells graded for SA-β-Gal staining in MUT and WT mice at 5 and 14 months. Data are mean ± SEM.

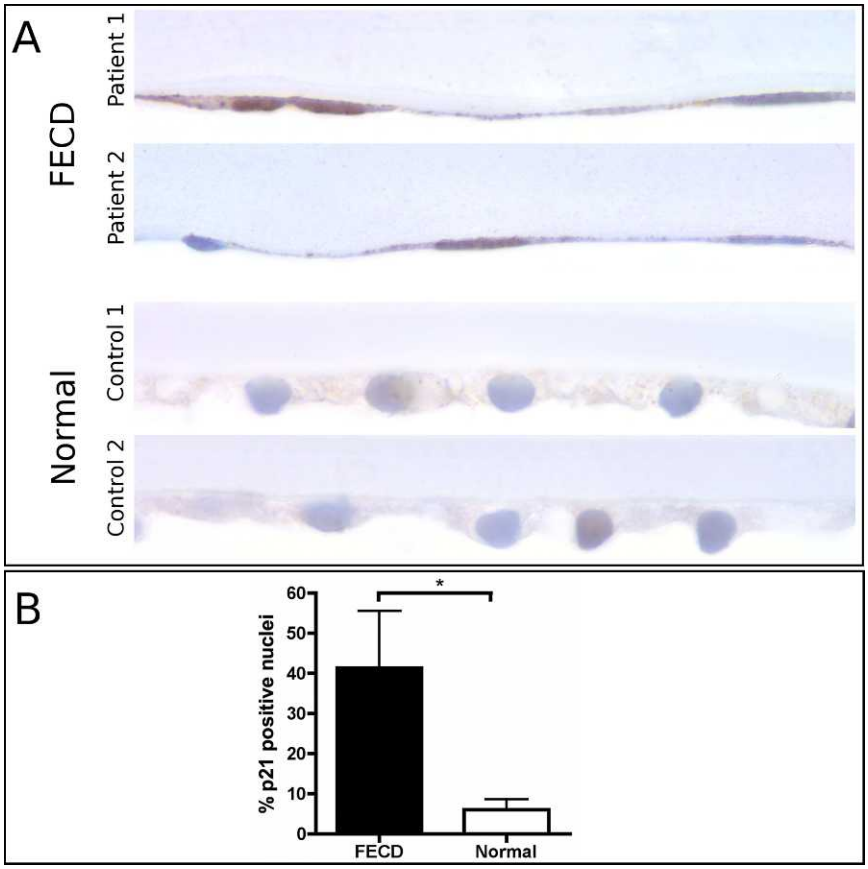


**Figure 6.** Immunohistochemical staining for p21 in tissue sections from paraffin-embedded human corneas. (**A**) Microscopic images of two p21-stained Fuchs endothelial corneal dystrophy and normal cases, respectively, magnification 1000×. (**B**) Quantitative analysis indicated a statistically significant increase in the number of p21 positive nuclei in FECD compared with normal endothelium. Data are mean ± SEM. $^{*}P < 0.05$.

nuclei evaluated was 40.2 ± 5.1 per FECD specimen and 183.0 ± 33.3 per autopsy globe.

## Discussion

The present study sought to generate an endothelial gene expression profile focusing on cellular stress response-related targets in the first *Col8a2* Q455K mutant knock-in mouse model for early-onset Fuchs Dystrophy.[12] We found in corneal endothelial cells from young (5 month) and mid-aged (10–14 months) homozygous *Col8a2*$^{Q455K/Q455K}$ knock-in mice essential characteristics of cellular senescence. These include: a senescence-like morphology with enlarged cell bodies, irregular shape, and an increased proportion of multinucleated cells; statistically significant transcriptional upregulation of senescence-associated genes *Cdkn1a* (*p21*), *Serpine1* (*PAI-1*), *Tagln* (*Sm22*), *Fn1*, and *Clu* (*ApoJ*); increased nuclear protein expression of p21 and its transcription factor p53; and an increased proportion of SA-β-Gal–positive cells. Furthermore, immunohistochemistry in human tissues indicates nuclear overexpression of the senescence associated protein p21 in the corneal endothelium of genetically undifferentiated FECD patients. Previous reports have clearly defined the central role of cellular stress in the pathogenesis of FECD and have elaborated the relationship between cellular stress and premature senescence in normal aging CECs.[9,10,12,14–16] Supported by these findings, the results presented herein provide new evidence suggesting that p21 overexpression and premature senescence are parts of the cellular stress response in the pathogenesis of both early- and late-onset FECD.

Cyclin dependent kinase inhibitors (CDKIs) play a central role in cellular senescence. Their expression in the corneal endothelium has been extensively studied.[17–19,24] In CECs, p16 and p21 seem to underlie an age-dependent regulatory mechanism and their inhibitory effect on cell cycle progression increases over time.[17,18] Various forms of cellular stress may induce p21 which is a main target of p53-mediated cell cycle arrest. To our great interest, p53 protein has recently been found to be overexpressed in human FECD endothelium.[25] Transcriptional upregulation is not essential for p53 activation and p53-mediated senescence, and this may explain why *Trp53* mRNA levels showed no statistically significant differences between MUT and WT mice in our array analysis.[26] However, we were able to detect increased nuclear localization of p53 protein in MUT corneal endothelium.

The upregulation of cell cycle inhibitor *Cdkn1a* (p21*)* was paralleled by the overexpression of cellular growth and cell cycle progression associated genes *Egr1*, *Ccnd1*, and *E2f1*. The coexpression of mitogenic stimuli and CDKIs as indicated by high coexpression of *Ccnd1* and *Cdkn1a* has been previously described in the context of cellular senescence.[27,28] This kind of costimulation causes a block of the cell cycle and simultaneously induces cellular growth, creating a state of hypertrophic growth arrest that lacks the ability of compensation by cell division and resulting in senescence induction.[29] In the context of FECD, this process could explain the response of remaining viable cells to enlarge (i.e. hypertrophy) in order to maintain an intact CEC monolayer as neighboring cells die. If so, then removing the cell cycle block (here p21)—

as it was demonstrated by Joyce and Harris in a similar concept—and allowing CEC proliferation even temporarily arises as a potentially intriguing treatment approach for FECD.[30]

*Cdkn1a/p21* is an important marker of cellular senescence and finds itself among a cluster of genes that are differentially expressed in senescent cells.[26] Further studies are needed to fully understand the roles of these individual cluster components in vivo.[26] However, it becomes increasingly evident that the changed gene expression leads to an impaired cellular function and altered production of molecules such as reactive oxygen species, growth factors, growth inhibitors, proteases, and extracellular matrix, which may also affect the neighboring cells and the tissue homeostasis.[26] *Serpine1* (*PAI-1*), *Tagln* (*Sm22*), *Fn1*, and *Clu* (*ApoJ*) are characteristic genes known to be upregulated in both replicative and premature senescence in addition to *Cdkn1a*.[20,21,31,32] Clusterin mRNA-levels were significantly upregulated in young 5-month-old mice and all genes showed statistically significant overexpression in 12-month MUT compared with WT animals. Interestingly, human FN1 and CLU have already previously been associated with FECD.[33,34] In addition, *CLU* gene variations were recently associated with Australian FECD patients, suggesting not only a secondary but also a primary role for *CLU*.[33,35] Zhang et al. demonstrated that fibronectin (FN1), a component of the ECM, accumulates in the DM of patients with early-onset FECD and assumed an abnormal production of fibronectin enriched ECM by affected CECs.[34]

Previous investigations from our laboratory suggest that stress of the endoplasmic reticulum may lead to an activation of the Unfolded Protein Response (UPR) in FECD.[9,12] These reports demonstrate UPR-upregulation in human late-onset FECD samples and the *Col8a2* Q455K mutant mouse model.[9,12] Therefore, a direct relationship between mutant *Col8a2*, the UPR, and increased p21 is a tempting speculation. Little is known about the interaction of the UPR with p21 expression, although one report describes a similar association between the UPR mediator CHOP and increased expression of the CDKIs, p16, p21, and p27, in human prostate cancer cells treated with the antitumor agent N-butylidenephthalide.[36] However, additional studies are required to directly demonstrate that UPR activation, either primarily or in addition to other forms of cell stress, is responsible for the upregulation of p21 described here in mouse and human forms of FECD.

In conclusion, this study provides first evidence for p21 upregulation and premature senescence in FECD. It may be assumed that CECs in FECD become senescent in order to overcome extended periods of different kinds of subcytotoxic cellular stress and/or in the context of cellular enlargement in order to maintain an intact monolayer. Ultimately, these compensatory mechanisms are insufficient to preserve tissue function, and vision loss ensues.

## *Acknowledgments*

The authors thank Jennifer Elisseeff, PhD, Norman Barker, MS, MA, RBP, Bonnie Gamblicher, and Jessica Hicks for technical assistance and the Wilmer Microscopy Core Facility.

## *References*

1. Biswas S, Munier FL, Yardley J, et al. Missense mutations in COL8A2, the gene encoding the alpha2 chain of type VIII collagen, cause two forms of corneal endothelial dystrophy. *Hum Mol Genet*. 2001;10:2415–2423.
2. Gottsch JD, Sundin OH, Liu SH, et al. Inheritance of a novel COL8A2 mutation defines a distinct early-onset subtype of Fuchs corneal dystrophy. *Invest Ophthalmol Vis Sci*. 2005;46:1934–1939.
3. Mok JW, Kim HS, Joo CK. Q455V mutation in COL8A2 is associated with Fuchs' corneal dystrophy in Korean patients. *Eye (Lond)*. 2009;23:895–903.
4. Vithana EN, Morgan PE, Ramprasad V, et al. SLC4A11 mutations in Fuchs endothelial corneal dystrophy. *Hum Mol Genet*. 2008;17:656–666.
5. Baratz KH, Tosakulwong N, Ryu E, et al. E2-2 protein and Fuchs's corneal dystrophy. *N Engl J Med*. 2010;363:1016–1024.
6. Riazuddin SA, Vithana EN, Seet LF, et al. Missense mutations in the sodium borate cotransporter SLC4A11 cause late-onset Fuchs corneal dystrophy. *Hum Mutat*. 2010;31:1261–1268.
7. Riazuddin SA, Zaghloul NA, Al-Saif A, et al. Missense mutations in TCF8 cause late-onset Fuchs corneal dystrophy and interact with FCD4 on chromosome 9p. *Am J Hum Genet*. 2010;86:45–53.
8. Riazuddin SA, Parker DS, McGlumphy EJ, et al. Mutations in LOXHD1, a recessive-deafness locus, cause dominant late-onset Fuchs corneal dystrophy. *Am J Hum Genet*. 2012;90:533–539.
9. Engler C, Kelliher C, Spitze AR, Speck CL, Eberhart CG, Jun AS. Unfolded protein response in Fuchs endothelial corneal dystrophy: a unifying pathogenic pathway? *Am J Ophthalmol*. 2010;149:194–202. e192.
10. Jurkunas UV, Bitar MS, Funaki T, Azizi B. Evidence of oxidative stress in the pathogenesis of fuchs endothelial corneal dystrophy. *Am J Pathol*. 2010;177:2278–2289.
11. Wang Z, Handa JT, Green WR, Stark WJ, Weinberg RS, Jun AS. Advanced glycation end products and receptors in Fuchs' dystrophy corneas undergoing Descemet's stripping with endothelial keratoplasty. *Ophthalmology*. 2007;114:1453–1460.
12. Jun AS, Meng H, Ramanan N, et al. An alpha 2 collagen VIII transgenic knock-in mouse model of Fuchs endothelial corneal dystrophy shows early endothelial cell unfolded protein response and apoptosis. *Hum Mol Genet*. 2012;21:384–393.
13. Ben-Porath I, Weinberg RA. The signals and pathways activating cellular senescence. *Int J Biochem Cell Biol*. 2005;37:961–976.
14. Mimura T, Joyce NC. Replication competence and senescence in central and peripheral human corneal endothelium. *Invest Ophthalmol Vis Sci*. 2006;47:1387–1396.
15. Konomi K, Joyce NC. Age and topographical comparison of telomere lengths in human corneal endothelial cells. *Mol Vis*. 2007;13:1251–1258.
16. Joyce NC, Zhu CC, Harris DL. Relationship among oxidative stress, DNA damage, and proliferative capacity in human corneal endothelium. *Invest Ophthalmol Vis Sci*. 2009;50:2116–2122.
17. Song Z, Wang Y, Xie L, Zang X, Yin H. Expression of senescence-related genes in human corneal endothelial cells. *Mol Vis*. 2008;14:161–170.
18. Enomoto K, Mimura T, Harris DL, Joyce NC. Age differences in cyclin-dependent kinase inhibitor expression and rb hyperphosphorylation in human corneal endothelial cells. *Invest Ophthalmol Vis Sci*. 2006;47:4330–4340.
19. Xiao X, Wang Y, Gong H, Chen P, Xie L. Molecular evidence of senescence in corneal endothelial cells of senescence-accelerated mice. *Mol Vis*. 2009;15:747–761.
20. Yu AL, Fuchshofer R, Kook D, Kampik A, Bloemendal H, Welge-Lussen U. Subtoxic oxidative stress induces senescence in retinal pigment epithelial cells via TGF-beta release. *Invest Ophthalmol Vis Sci*. 2009;50:926–935.
21. Yu AL, Birke K, Moriniere J, Welge-Lussen U. TGF-{beta}2 induces senescence-associated changes in human trabecular

meshwork cells. *Invest Ophthalmol Vis Sci*. 2010;51:5718–5723.

22. Dimri GP, Lee X, Basile G, et al. A biomarker that identifies senescent human cells in culture and in aging skin in vivo. *Proc Natl Acad Sci U S A*. 1995;92:9363–9367.
23. Kurz DJ, Decary S, Hong Y, Erusalimsky JD. Senescence-associated (beta)-galactosidase reflects an increase in lysosomal mass during replicative ageing of human endothelial cells. *J Cell Sci*. 2000;113(Pt 20):3613–3622.
24. Joyce NC. Cell cycle status in human corneal endothelium. *Exp Eye Res*. 2005;81:629–638.
25. Azizi B, Ziaei A, Fuchsluger T, Schmedt T, Chen Y, Jurkunas UV. p53-regulated increase in oxidative-stress–induced apoptosis in Fuchs endothelial corneal dystrophy: a native tissue model. *Invest Ophthalmol Vis Sci*. 2011;52:9291–9297.
26. Muller M. Cellular senescence: molecular mechanisms, in vivo significance, and redox considerations. *Antioxid Redox Signal*. 2009;11:59–98.
27. Zhuo L, Cai G, Liu F, et al. Expression and mechanism of mammalian target of rapamycin in age-related renal cell senescence and organ aging. *Mech Ageing Dev*. 2009;130:700–708.
28. Blagosklonny MV. Cell senescence: hypertrophic arrest beyond the restriction point. *J Cell Physiol*. 2006;209:592–597.
29. Demidenko ZN, Blagosklonny MV. Growth stimulation leads to cellular senescence when the cell cycle is blocked. *Cell Cycle*. 2008;7:3355–3361.
30. Joyce NC, Harris DL. Decreasing expression of the G1-phase inhibitors, p21Cip1 and p16INK4a, promotes division of corneal endothelial cells from older donors. *Mol Vis*. 2010;16:897–906.
31. Debacq-Chainiaux F, Pascal T, Boilan E, Bastin C, Bauwens E, Toussaint O. Screening of senescence-associated genes with specific DNA array reveals the role of IGFBP-3 in premature senescence of human diploid fibroblasts. *Free Radic Biol Med*. 2008;44:1817–1832.
32. Matos L, Gouveia A, Almeida H. Copper ability to induce premature senescence in human fibroblasts. *Age (Dordr)*. 2011;34:783–794.
33. Jurkunas UV, Bitar MS, Rawe I, Harris DL, Colby K, Joyce NC. Increased clusterin expression in Fuchs' endothelial dystrophy. *Invest Ophthalmol Vis Sci*. 2008;49:2946–2955.
34. Zhang C, Bell WR, Sundin OH, et al. Immunohistochemistry and electron microscopy of early-onset fuchs corneal dystrophy in three cases with the same L450W COL8A2 mutation. *Trans Am Ophthalmol Soc*. 2006;104:85–97.
35. Kuot A, Hewitt AW, Griggs K, et al. Association of TCF4 and CLU polymorphisms with Fuchs' endothelial dystrophy and implication of CLU and TGFBI proteins in the disease process. *Eur J Hum Genet*. 2012;20:632–638.
36. Chiu SC, Chen SP, Huang SY, et al. Induction of apoptosis coupled to endoplasmic reticulum stress in human prostate cancer cells by n-butylidenephthalide. *PLoS One*. 2012;7:e33742.